Atmos. Chem. Phys. Discuss., 14, 435–469, 2014
www.atmos-chem-phys-discuss.net/14/435/2014/
doi:10.5194/acpd-14-435-2014

Atmospheric Chemistry and Physics Discussions

An alternative method estimating hygroscopic growth factor of aerosol light scattering coefficient: a case study in an urban area of Guangzhou, South China

Z. J. Lin[1], Z. S. Zhang[1], L. Zhang[2], J. Tao[1], R. J. Zhang[3], J. J. Cao[4], and Y. H. Zhang[5]

[1]South China Institute of Environmental Sciences (SCIES), Guangzhou, China
[2]Air Quality Research Division, Science Technology Branch, Environment Canada, Toronto, Canada
[3]RCE-TEA, Institute of Atmospheric Physics, Chinese Academy of Sciences, Beijing, China
[4]Key Laboratory of Aerosol, SKLLQG, Institute of Earth Environment, Chinese Academy of Sciences, Xi'an, China
[5]State Joint Key Laboratory of Environmental Simulation and Pollution Control, College of Environmental Sciences and Engineering, Peking University, Beijing, China

Received: 11 December 2013 – Accepted: 17 December 2013 – Published: 7 January 2014

Correspondence to: J. Tao (taojun@scies.org)

Published by Copernicus Publications on behalf of the European Geosciences Union.

ACPD
14, 435–469, 2014

Abstract

A method was developed to estimate hygroscopic growth factor (f(RH)) of aerosol light scattering coefficient (b_{sp}), making use of the measured size- and chemically-resolved aerosol samples. Regarding this method, chemical composition of the measured aerosol samples were first reconstructed using the equilibrium model ISOPPORIA II. The model reconstructed chemical composition varies with a varying relative humidity (RH) input, which was then employed to calculate b_{sp} and f(RH) of b_{sp} using Mie Model. Further, the RH dependence of f(RH) of b_{sp} (denoted as f_{sp}(RH)) derived from model calculation was empirically fitted with a two-parameter formula. One of the two parameters was set to be a constant for practical applications. For validation, the developed formula of f_{sp}(RH) was applied to correct the long-term records of measured b_{sp} from the values under comparative dry conditions to the ones under ambient RH conditions. Compared with the original b_{sp} data, the f(RH)-corrected b_{sp} had a higher linear correlation with and a smaller discrepancy from the b_{sp} data derived directly from visibility and absorption measurements. The method described in this paper provides an alternative approach to estimate f_{sp}(RH) and has many potential applications.

1 Introduction

Atmospheric aerosols influence radiation budget of the Atmosphere–Earth system through light scattering and absorption, which impact climate and degrade air visibility (Seinfeld and Pandis, 2006). Aerosol light scattering coefficient (b_{sp}) increases with increasing relative humidity (RH) due to hygroscopic growth of water-soluble fractions of ambient aerosols (Malm et al., 2003; Xu et al., 2002). Thus, high RH may cause larger single particle scattering albedo (ω_0) according to Mie Theory, and as a result, a potential cooling effect on climate. Besides, air visibility degradation could be strengthened in areas with wet climate and high aerosol loading.

ACPD
14, 435–469, 2014

Knowledge of aerosol chemical composition is needed for calculating b_{sp} under a desired RH environment with Mie model (Seinfeld and Pandis, 2006). Accordingly, the hygroscopic growth of b_{sp} could be determined. Thermodynamic equilibrium models such as E-AIM (Wexler and Clegg, 2002) and ISOPPORIA II (Fountoukis and Nenes, 2007) have thus been developed for the purpose of reconstructing aerosol chemical composition with varying RH. These models take advantage of some pure species' hygroscopic growth factor (Tang and Munkelwitz, 1994; Tang, 1996, Tang et al., 1997) established by laboratory measurement and numerical parameterization studies. On the other hand, the hygroscopic growth factor of b_{sp} (f_{sp}(RH)) can be estimated through simultaneous measurement of b_{sp} of both dry and ambient aerosols, the latter is in equilibrium in ambient RH environment, using Nephelometers (Malm et al., 2003; Xu et al., 2002).

In the Pearl River Delta region of South China, air visibility degradation, the so called Haze problem mainly caused by severe aerosol pollution, has attracted attentions of public and the scientific community (Wu et al., 2005). Intensive haze episodes sometimes happened along with wet weather, which suggests the necessity of assessing the impact of high RH environment on haze formation. Recently, a series of field experiments have been conducted in this region to understand aerosol optical properties and relevant hygroscopic behavior. Among these, one experiment was carried out during November 2004 at Xinken (Cheng et al., 2008a, b; Y. H. Zhang et al., 2008), a suburban area of Guangzhou, in which parallel measurements with HDMPS, TDMPS and MOUDI were employed to determine the size-dependent hygroscopic growth factor and optical refractive index. RH dependent of aerosol optical properties were then calculated using Mie Model. Another experiment was conducted in July 2006 inside the urban area of Guangzhou to derive b_{sp} from visibility and absorption measurements and to compare with the Nephelometer measured ones in order to investigate the RH dependence of b_{sp} (Liu et al., 2008). Although these two studies illustrated the methods of estimating the hygroscopic growth of b_{sp}, the first one relied on a combination of complicated instruments which is not practical for long-term investigation, while the second one could

ACPD
14, 435–469, 2014

not be utilized to examine the impact of chemical species on hygroscopic behavior of aerosols population. During 2009 and 2010, continuous experiments were conducted at the observation site of the South China Institute of Environmental Science (SCIES) located in an urban area of Guangzhou. Based on these experiments, chemical composition of $PM_{2.5}$ and particles number size distribution measured by APS were integrated into Mie model calculation in order to develop a practical method to estimate the hygroscopic behavior of b_{sp}(Lin et al., 2013). Results suggested that an accurate description of particles number size distribution is the key factor to improve the method's performance.

However, f_{sp}(RH) introduced by the studies mentioned above needs to be further validated with long-term observation results. For this purpose and for further development of a practical method estimating f_{sp}(RH), the size- and chemically-resolved aerosol samples collected in 2010 were utilized in the present study. The developed f_{sp}(RH) was applied to correct the long-term Nephelometer measured b_{sp} during 2008 to 2010 and was validated through a comparison with values derived from visibility and absorption measurements. In addition, the contribution of RH to the enhancement of b_{sp} and ω_0 in the urban area of Guangzhou was quantified based on f_{sp}(RH).

2 Methods

2.1 Experimental

The SCIES observation site (23°70′ N, 113°210′ E) is situated in the downtown area of Guangzhou city. All instruments were installed on the roof of a building about 53 m above the ground. This site is built with a clear vision over 300°, around which there are residential buildings and a park about 500 m to the northeast. There is no obvious air pollution source within a circumference of 3 km except mobile emissions. Figure 1 depicts the site location and surroundings. At this field site, fine particles concentra-

ACPD
14, 435–469, 2014

tion and aerosol optical properties, as well as gaseous pollutants and meteorological parameters, have been recorded and studied since 2005 (Tao et al., 2009, 2012, 2014).

For the current study, size-segregated aerosols were collected by a high flow cascade impactor (MSP Co., USA) with the particle cut-sizes at 10, 2.5, 1.4, 1.0, 0.44, and 0.25 µm. It was operated at a flow rate of 100 L min^{-1} for approximately 24 h to collect one set of filter samples. The samplings were performed during May to June (4, 8, 12, 16, 20, 24, 26 May; 5, 12, 18 June) and November to December (12, 14, 16, 18, 20, 22, 24, 26, 28, 30 November; 2, 4, 6, 8 December) in 2010, with the former period stands for a wet season (WS) and the latter for a dry season (DS) in South China. OC and EC were measured by a carbon analyzer following the NIOSH 5040 protocol. Major water-soluble inorganic cations (Na^+, NH_4^+, K^+, Mg^{2+} and Ca^{2+}) and anions (SO_4^{2-}, NO_3^-, and Cl^-) were detected by a Dionex ICS-3000 ion chromatograph. The cations were separated on an Ionpac CS12 analytical column with CG12 guard column using 20mM methane-sulfonic acid as eluent, while the anions were separated on Ionpac AS14 and AG14 columns with a mixture of 4.5 mM Na_2CO_3 and 1.4 mM $NaHCO_3$as eluent. More details on the chemical analysis procedures mentioned above were described in a previous study (Zhang et al., 2013).

BC was measured using an Aethalometer (Magee Scientific Company, Berkeley, CA, USA, Model AE-31) with a flow rate of 5 L min^{-1}. The sampling air passed through a $PM_{2.5}$ inlet and a drying tube (RH ≤ 40 %) before entering into AE-31. The instrument was calibrated to zero by replacing the old filter in the canister inlet with a clean one every week. NO_2 was measured by Thermo 42i gas analyzer. b_{sp} was measured by TSI 3563 Nephelometer. Calibration of Nephelometer was performed by carbon dioxide (CO_2) as high-span gas and filtered air as low-span gas. The instrument drew ambient air through a temperature-controlled inlet at a flow rate of 20 L min^{-1}.

Meteorological parameters including visibility (VIS), RH, pressure (PRES) and temperature (TEMP) were measured every 30 min. Visibility was measured using a present weather detector (VAISALA Company, Helsinki, Finland, Model PWD22). Ambient RH, PRES and TEMP were measured by the corresponding probe (VAISALA Company,

ACPD
14, 435–469, 2014

Helsinki, Finland, model QMH102). Both meteorological instruments were mounted at 3 m above the platform of the observation site. Experimental details including uncertainties caused by field measuring and laboratory chemical analysis are summarized in Table 1.

2.2 Reconstruction of aerosol chemical composition using ISOPPORIA II model

Taking mass concentration of the measured water-soluble ions as input, the thermodynamic model ISOPPORIA II (Fountoukis and Nenes, 2007) was used to reconstruct the chemical composition of aerosol samples which were considered to compose of supersaturated solution droplets. The model was setup to solve a "Reverse" problem with the output being set to be in the state of "metastable". The recorded RH and TEMP were also needed as model input. The aqueous species (Na^+, NH_4^+, Ca^{2+}, K^+, Mg^{2+}, HSO_4^-, SO_4^{2-}, NO_3^- and Cl^-) in the model output were associated with each other in the form of chemical compounds according to the abundance of SO_4^{2-} in aerosols (Fountoukis and Nenes, 2007). The extent of SO_4^{2-} abundance and the corresponding potential compounds are described in Table 2. If any portion of NO_3^- or Cl^- remained, they were treated as HNO_3 or HCl, respectively. $CaSO_4$ was assumed to be completely insoluble.

Mass concentration of OM was estimated as 1.6 times of OC (Cao et al., 2007; Xing et al., 2013). Unlike water-soluble components, the water uptake by OM was not considered here due to the lack of (1) adequate data for the speciation of WSOC and (2) the accurate RH dependence curve for OM. Neither EC was assumed to undergo hygroscopic growth.

2.3 Calculation of b_{sp} using Mie model

The reconstructed chemical composition described in Sect. 2.2 was then used to calculate b_{sp} based on Mie theory. Optical properties of aerosol population can be calculated with particles number concentration and the scattering/absorption efficiency of

ACPD
14, 435–469, 2014

a single particle (Bohren and Huffman, 1998). Three different assumptions of particles mixing state (Bond and Bergstrom, 2005; Seinfeld and Pandis, 2006) are concerned here, which are "Internal Mixed (volume averaged)", "External Mixed" and "Core–Shell mixed (encapsulated)" (denoted below as subscript int, ext, cs, respectively). The formulas for these mixing states are described respectively by Eqs. (1)–(3) where the subscripts i and j denote the ith chemical component and the jth stage of particle size, respectively.

$$b_{\mathrm{sp/ap,int}} = \sum_j \frac{\pi D_j^2}{4} \cdot Q_{\mathrm{sp/ap,int}} \left(\lambda, D_j, \sum_i \alpha_{i,j} m_i \right) \cdot N_j \quad (1)$$

$$b_{\mathrm{sp/ap,ext}} = \sum_j \sum_i \frac{\pi D_j^2}{4} \cdot Q_{\mathrm{sp/ap,ext},i,j} \left(\lambda, D_j, m_i \right) \cdot N_{i,j} \quad (2)$$

$$b_{\mathrm{sp/ap,cs}} = \sum_j \frac{\pi D_j^2}{4} \cdot Q_{\mathrm{sp/ap,cs}} \left(\lambda, D_{j,c}, D_{j,s}, m_{j,c}, \sum_i \alpha_{i,j,s} m_{i,s} \right) \cdot N_j \quad (3)$$

The calculation of $Q_{\mathrm{sp/ap}}$ that was needed in the above equations was described in literatures (Bohren and Huffman, 1998). The parameter λ is the light wavelength and was set at 550 nm throughout this work. D is the particle's stoke diameter and was calculated based on the median cutting diameter (D_a) of the particle sampler and the particle density (ρ) (see Eq. 4 below). N is the particles number concentration and was calculated using Eq. (5). $C_{i,j}$ in Eqs. (5) and (6) refers to mass concentrations of reconstructed chemical components. α is the volume fraction and was calculated using Eq. (6). m ($= n + ki$) is the optical refractive index (ORI). Values of ρ and m were stated in a previous paper (Lin et al., 2013) and are also listed here in Table 3. Corresponding computational codes (Bohren and Huffman, 1998) were integrated into MATLAB script

ACPD
14, 435–469, 2014

for batch processing

$$D = D_a \cdot \frac{1}{\sqrt{\rho}} \tag{4}$$

$$N_{i,j} = \frac{6 \cdot C_{i,j}}{\pi \cdot D_j^3 \cdot \rho_i} \tag{5}$$

$$\alpha_{i,j} = \frac{C_{i,j}}{\rho_i} / \sum_i \frac{C_{i,j}}{\rho_{i,j}} \tag{6}$$

2.4 Parameterization of f_{sp}(RH)

The water-soluble fractions of aerosol particles, such as ammonia sulfate and sodium chloride, absorb more water in high RH environment. Thus, aerosol chemical composition varies with RH, and the density and ORI of aerosol particles change accordingly. The input of RH in ISOPPORIA II can be varied in a desired range, and chemical composition at a certain RH state can be determined by the model. This illustrates a way to simulate RH dependence of b_{sp} based on Mie model making use of ISOPPORIA II determined aerosol chemical composition.

f_{sp}(RH) is the ratio of b_{sp}(RH) to b_{sp}(RH$_0$), where RH$_0$ refers to a RH condition under which aerosols are considered to be too dry to grow. Usually, f_{sp}(RH) was fitted by some of the well-known empirical curves (Cheng et al., 2008b) noted as Eqs. (7)–(9).

$$f_{sp}(\mathrm{RH}) = \left(\frac{1-\mathrm{RH}}{1-\mathrm{RH}_0}\right)^{-a} \tag{7}$$

$$f_{sp}(\mathrm{RH}) = \left(\frac{1-\mathrm{RH}}{1-\mathrm{RH}_0}\right)^{-a\cdot\mathrm{RH}} \tag{8}$$

$$f_{sp}(\mathrm{RH}) = \left(\frac{1-\mathrm{RH}}{1-\mathrm{RH}_0}\right)^{-a\cdot(\mathrm{RH}-\mathrm{RH}_0)} \tag{9}$$

ACPD
14, 435–469, 2014

As mentioned above, the output of ISOPPORIA II is at the state of "metastable", which allows particles to absorb water at low ambient RH conditions. RH as low as 0.12 was recorded at our site during the experiment period, and thus the value of 0.10 was used for RH_0.

Among the three empirical curves, Eq. (8) seemed to best describe our data, but it underestimated the growth of f_{sp} when RH was below 0.7. To correct this problem, Eq. (8) was modified to Eq. (10) by introducing a second parameter "b".

$$f_{sp}(RH) = \left(\frac{1 - RH}{1 - RH_0}\right)^{-a\cdot(RH+b)} \quad (10)$$

2.5 Validation of f_{sp}(RH)

Aerosols drawn into Nephelometer was heated for the purpose of RH control, so that b_{sp} measured by Nephelometer could be corrected to its hygroscopic state in ambient with f_{sp}(RH). Equation (11) describes this correction, where $b_{sp,cal}$ stands for the b_{sp} corrected with f_{sp}(RH).

$$b_{sp,cal}(RH_{amb}) = b_{sp}(RH_{nep}) \cdot \frac{f_{sp}(RH_{amb})}{f_{sp}(RH_{nep})} \quad (11)$$

Before the correction with Eq. (11), Nephelometer measured b_{sp} was corrected for Angular Nonidealities following the method presented in a previous paper (Anderson and Ogren, 1998).

On the other hand, b_{sp} can be estimated by Eq. (12) based on visibility and absorption measurements (Seinfeld and Pandis, 2006) and is denoted as $b_{sp,mea}$ below.

$$b_{sp,mea} = b_{ext,mea} - b_{ap,mea} - b_{ag,mea} - b_{sg,mea} \quad (12)$$

In Eq. (12), $b_{ext,mea}$ represents the total light extinction coefficient and was derived from air visibility following Eq. (13) which is stated in the users' manual of PWD22. $b_{ag,\,mea}$

ACPD
14, 435–469, 2014

represents the light absorption by gaseous pollutant and was practically estimated by mass concentration of NO_2 following Eq. (14) (Pitchford et al., 2007).

$$b_{\text{ext,mea}} = \frac{3}{\text{visibility}} \tag{13}$$

$$b_{\text{ag,mea}} = 330 \cdot 22.4 \cdot \frac{C_{NO_2}}{M_{NO_2}} \tag{14}$$

C_{NO_2} and M_{NO_2} in Eq. (14) are mass concentration and molecular weight of NO_2, respectively. Light scattering by air, denoted as $b_{\text{sg,mea}}$, was calculated with Eq. (15) (Seinfeld and Pandis, 2006). Mass concentration of BC, $C_{\text{bc,880 nm}}$, was used to estimate particles light absorption coefficient $b_{\text{ap,mea}}$ following a linear relationship as Eq. (16) (Wu et al., 2009).

$$b_{\text{sg,mea}} = 11.4 \cdot \frac{293}{\text{TEMP}} \cdot \text{PRES} \tag{15}$$

$$b_{\text{ap,mea}} = 8.28 \cdot C_{\text{bc,880 nm}} + 2.23 \tag{16}$$

The correlation analysis between $b_{\text{sp,cal}}$ and $b_{\text{sp,mea}}$ using linear regression was also carried out and was considered to be an validation of $f_{\text{sp}}(\text{RH})$. Statistical results of the fundamental data involved in this validation are shown in Table 4.

2.6 Uncertainties

Potential sources of uncertainties delivered from field measurement and laboratory analysis are listed in Table 1. In addition, ORI of EC also contributed to the total uncertainty, with the real part contributing 3.00 % and the imaginary part, 5.00 % (Cheng et al., 2008b). As a result, the total uncertainty of this study was calculated to be 9.36 %

ACPD
14, 435–469, 2014

with Eq. (17) where U_i refers to the ith source of uncertainty.

$$U_{\text{total}} = \left(\sum_i U_i^2 \right)^{1/2} \quad (17)$$

3 Results and discussion

3.1 Reconstructed aerosol chemical composition

Measured inorganic ions were needed as model input for ISOPPORIA II to reconstruct aerosol chemical composition. The ions used here, as well as OC and EC, were collected during May–June and November–December of 2010. At first, the data was briefly examined to ensure the data quality (Fig. 2). A strong linear correlation was found between the total of the Cations ($[Na^+]/23 + [NH_4^+]/18 + [Ca^{2+}]/40 \cdot 2 + [Mg^{2+}]/24 \cdot 2 + [K^+]/39$) and the total of Anions ($[SO_4^{2-}]/96 \cdot 2 + [NO_3^-]/62 + [Cl^-]/35.5$) in each particle size range (Fig. 2a). A slope of 1.0 was found from the linear regression, indicating the electronic charge balance among the ions. The charge balance warranted the ISOPPORIA II model to reconstruct the chemical composition at a reasonable accuracy. The mass concentration of ions peaked in size ranges of 0.44–1 µm and 2.5–10 µm, which can be explained by the different dominant ions in different size ranges (e.g., L. Zhang et al., 2008).

The linear correlation between OC and EC is shown in Fig. 2b. Note that the mass of OC and EC in the size range of 10–18 µm was not weighed in laboratory and thus was not shown in Fig. 2b. EC and OC had the higher correlation in the size ranges of 0.44–1 µm and 2.5–10 µm than in other size ranges, with the correlation coefficient being 0.73 and 0.58, respectively. EC had lower concentrations than OC in most samples of the size range > 0.25 µm, but much higher concentrations than OC in all the samples of the size range < 0.25 µm.

ACPD
14, 435–469, 2014

The reconstructed aerosol chemical composition was discussed below; but it should first be noted that the total mass of each aerosol sample used through this study is the sum of all the determined chemical components. The unidentified components were initially assumed to be negligible in mass and light scattering compared to the determined ones.

The reconstructed aerosol chemical composition in each size range is illustrated in Figs. 3 and 4. The major chemical compounds associated by ISOPPORIA II include $(NH_4)_2SO_4$, Na_2SO_4, NH_4NO_3, $NaNO_3$, K_2SO_4, $CaSO_4$, $Ca(NO_3)_2$, Water, OC and EC. As illustrated in Fig. 3, they accounted for about 95 % of the total mass. Overall, inorganic salts accounted for 40–50 % of the total mass in particles larger than 0.44 µm and a bit less in smaller particles. In contrast, OC and EC contributed about 30–50 % in particles smaller than 0.44 µm and less than 30 % in larger particles. Calcium salts and $NaNO_3$ were mostly in coarse particles, while ammonia salts, Na_2SO_4 and K_2SO_4 were in fine ones.

The mass fraction of each major compound differed between the wet and dry season with the distinct difference for water content. The mass fraction of K_2SO_4 apparently increased in the dry season compared to that in the wet season, while that of sodium salts decreased. Although the mass fraction of each major compound varied with season, size distribution of each major compound was similar between the two seasons (Fig. 4). Specifically, $(NH_4)_2SO_4$, Na_2SO_4 and K_2SO_4 peaked in the size range of 0.44–1.0 µm, $NaNO_3$, $CaSO_4$ and $Ca(NO_3)_2$ in 2.5 ~ 1.0 µm, and NH_4NO_3 and Water had two peaks of 0.44–1.0 µm and 2.5–1.0 µm.

3.2 b_{sp} of the mixed aerosol

ORI and density of aerosol particles are key factors influencing b_{sp}. They can be determined by the volume ratios of the reconstructed chemical constituents for mixed particles. ORI and density of internal mixed particles represent the integrated physical properties of the particle population and were illustrated in Fig. 5. Particles smaller than 0.44 µm generally had larger real and imaginary part of ORI than those in larger parti-

ACPD
14, 435–469, 2014

cles (Fig. 5a) due to the smaller water fractions in smaller particles (Fig. 3). Similarly, particle densities were also larger in smaller particles (Fig. 5b). On the other hand, the linear correlations between the real part of ORI and the density were weaker in smaller particles.

b_{sp} was calculated after inputting all the required parameters into Mie model. For validation, b_{sp} calculated by the model was compared with b_{sp} derived from visibility and absorption measurements. These two data set were in the same time periods during May–June and November–December of 2010 (Fig. 5c). The modeled b_{sp} had strong linear correlations with the measured b_{sp} with R^2 values larger than 0.85, regardless of the mixing state assumptions of the particles. However, the regression slopes deviated from 1.0 significantly and the model calculation only matched around 45 % of the measured magnitude. In a previous study we speculated two potential causes responsible for this discrepancy (Lin et al., 2013). The first cause could be due to a truncation error in the model calculation because the size range of each size-cutting stage of the employed aerosol sampler was too wide to attain particles number size distribution of high-resolution. Contributions of the unidentified chemical constituents to b_{sp} were still unknown, which accounted for the second cause.

Nevertheless, we could still take advantage of the computation method of f_{sp}(RH) to derive the RH dependence of f_{sp}(RH) considering the existence of the strong linear correlations between the model calculated and the measured b_{sp}. Besides, $b_{sp}(RH_0)$ and b_{sp}(RH) should both be subjected to the same type of truncation errors, which would eventually have minimum impact on the ratio f_{sp}(RH).

3.3 RH dependence curve of f_{sp}(RH)

To evaluate the effectiveness of Eq. (10) in curve fitting of f_{sp}(RH), three indexes are employed here including relative standard deviation (standard deviation divided by arithmetic average) of parameter "*a*" (RSDA), maximum total residual of curve fitting (MATR) and minimum R^2 value of curve fitting (MIRV).

ACPD
14, 435–469, 2014

Table 5 suggests that Eq. (10) performed better in curve fitting than Eq. (8) did with respect to a much smaller MATR and a higher MIRV. However, a two-parameter curve fitting with both parameters having large standard deviations is difficult for practical applications. In this regard, it was tried to determine the parameter "a" by setting parameter "b" to be a constant. The value of parameter "b" was tuning from 0.5 to 3 and with an increment of 0.05.

The tuning results show that RSDA slightly increased with increasing parameter "b", and reached its peak at about 9.5 %. Meanwhile, MATR dropped to the minimum value when parameter "b" was chosen as 1.90, 1.65 and 1.45 for internal mixed, external mixed and core-shell mixed particles, respectively. The high value (> 0.98) of MIRV further indicates the effectiveness of Eq. (10) with a constant parameter "b" in curve fitting of f_{sp}(RH). Consequently, the RH dependence curve of f_{sp}(RH) was determined with the corresponding parameters tabulated in Table 6.

Judged by Eq. (10), the exponent "$a \cdot (\mathrm{RH} + b)$" controls the growth rate of f_{sp}(RH). As shown in Fig. 5d, with a constant parameter "b", the variation of parameter "a" among aerosol samples had a connection with the variation of water-soluble salts' portion. The fact that water-soluble salts' portion here was with respect to dry aerosols. For external mixed particles, the linear correlation coefficient between parameter "a" and portion of water-soluble salts reached 0.83. It is evident that the portion of water-soluble salts affected f_{sp}(RH), and high water-soluble salts portion could accelerate the hygroscopic growth of b_{sp}.

Figure 6 illustrates RH dependence curve of f_{sp}(RH) determined in this study and compares with those reported in literatures. Although with discrepancies, the curves generated from the present study shared similar pattern with those in literatures. The relative accuracy of these curves can only be validated with high quality measurements of b_{sp} under various humidity conditions.

ACPD
14, 435–469, 2014

3.4 Validation and application of f_{sp}(RH)

To validate the f_{sp}(RH) formula generated in the present study, the Nephelometer measured b_{sp} was corrected with f_{sp}(RH) (referred to $b_{sp,cal}$) and compared with b_{sp} derived directly from visibility and absorption measurements (referred to $b_{sp,mea}$). As an example, f_{sp}(RH) of internal mixed particles (referred to $f_{sp,int}$ and depicted in Fig. 6) was used and results were presented here. The data of Nephelometer measurement covered the period of March 2008 to April 2010 and was grouped based on the month of the year to examine any possible seasonality. The number of validated data (NVD) in each month was in the range of 350–1450 (Fig. 7a). The monthly average ambient RH was in the range of 0.55–0.80, higher than those inside Nephelometer that was in the range of 0.40–0.65 (Fig. 7b).

A linear regression with zero intercept was used to correlate $b_{sp,cal}$ and $b_{sp,mea}$. Before applying f_{sp}(RH) correction to the Nephelometer measured b_{sp}, the correlation between $b_{sp,cal}$ and $b_{sp,mea}$ had an R^2 around 0.75 and a slope ranging between 0.50–0.90. With f_{sp}(RH) correction, R^2 was in a narrow range of 0.80–0.92 while the slope was in the range of 0.65–1.00. Notably, the slopes in August, September, November and December approached 1.00. Applying f_{sp}(RH) of external and Core–Shell mixed particles into the corresponding b_{sp} correction showed similar results as using f_{sp}(RH) of internal mixed particles. Obviously, the f_{sp}(RH) correction remarkably improved the correlation and the agreement between $b_{sp,cal}$ and $b_{sp,mea}$.

It is worth to mention that our observation site locates in a region with wet climate. Each aerosol sample inside Nephelometer was heated in order to keep the instrument properly functioning. As mentioned in Sect. 3.1, aerosols absorb more water during the wet season, thus the heating could drive off water and lower b_{sp} irreversibly. Besides, this study only considered the hygroscopic growth of water-soluble inorganic fractions, but not water-soluble fractions in OM. However, water-soluble fractions in OM could grow significantly when RH > 0.6 (Gysel et al., 2004). These two factors might be

ACPD
14, 435–469, 2014

the main causes of the discrepancies between $b_{sp,cal}$ and $b_{sp,mea}$ despite of including f_{sp}(RH)-correction during February and April.

On the basis of f_{sp}(RH), the enhancement of b_{sp} and ω_0 by RH can be quantified. The enhancement of b_{sp}, Δb_{sp}, is defined as the ratio of $f_{sp}(RH_{amb})$ to f_{sp}(RH = 40 %), while the enhancement of ω_0, $\Delta\omega_0$, is calculated as $(\omega_0(RH_{amb}) - \omega_0(RH = 40\,\%))/\omega_0(RH = 40\,\%)$. Note that ω_0 was derived from the visibility and absorption measurements.

As illustrated in Fig. 8, the enhancement of b_{sp} had two peaks respectively in February and June, and a valley in October. b_{sp} was strengthened by 1.45–1.75 times during January to August and 1.22–1.40 times from September to December. The enhancement of ω_0 stayed around 4 % from January to May, peaked up to about 7 % during June to August, and dropped to nearly 2 % in October before bouncing back to around 3 % in November and December.

4 Summary and conclusion

Making use of size- and chemically-resolved aerosol samples, the aerosol chemical composition under a desired RH environment was reconstructed using ISOPPORIA II model. The major chemical constituents were $(NH_4)_2SO_4$, Na_2SO_4, NH_4NO_3, $NaNO_3$, K_2SO_4, $CaSO_4$, $Ca(NO_3)_2$, water, OC and EC. The mass fraction of water and K_2SO_4 obviously differed between the wet and dry season. Despite the mass concentration varying with season, the mass size distribution of each major constituent showed a similar pattern between the two seasons. Calcium salts and $NaNO_3$ were mostly in coarse particles, while ammonia salts, Na_2SO_4 and K_2SO_4 were in fine ones. Aerosol optical properties were calculated by Mie model based on the reconstructed aerosol chemical composition. Modeled b_{sp} well correlated with measured b_{sp}, but was smaller by a factor of 2, which was probably caused by the truncation error delivered from the measured particles number size distribution of low-resolution.

ACPD
14, 435–469, 2014

The hygroscopic growth factor of b_{sp}, f_{sp}(RH), was determined based on model output of b_{sp} under desired RH conditions. The formula of f_{sp}(RH) was best described by a two-parameter empirical curve. However, one of the two parameters was set to be a constant for practical applications. The developed f_{sp}(RH) formula was then applied to correct the Nephelometer measured b_{sp}. With the f_{sp}(RH) correction, the linear correlation between Nephelometer measured b_{sp} and visibility derived b_{sp} was remarkably improved to a strong level, and the discrepancy between these two data set was reduced substantially. This validated the f_{sp}(RH) determined with the method described in present study. As an example of f_{sp}(RH) application, the enhancement of b_{sp} and ω_0 in ambient RH environment were assessed for the urban area of Guangzhou. Lessons learned from the current study include careful use of the heating procedure inside Nephelometer in future experiments since the heating could lower the b_{sp} irreversibly. Moreover, the contribution of hygroscopic growth of water-soluble organic fractions to f_{sp}(RH) needs further investigation.

Acknowledgements. This study was supported by the Special Scientific Research Funds for Environment Protection Commonweal Section (201409009) and the National Basic Research Program of China (2013FY112700).

References

Anderson, T. L. and Ogren, J. A.: Determining aerosol radiative properties using the TSI 3563 integrating nephelometer, Aerosol Sci. Tech., 29, 57–69, doi:10.1080/02786829808965551, 1998.

Bohren, C. F. and Huffman, D. R.: Absorption and Scattering of Light by Small Particles, John Wiley and Sons, Inc., New York, 1998.

Bond, T. C. and Bergstrom, R. W.: Light absorption by carbonaceous particles: an investigative review, Aerosol Sci. Tech., 39, 1–41, 2005.

Cao, J. J., Lee, S. C., Chow, J. C., Watson, J. G., Ho, K. F., Zhang, R. J., Jin, Z. D., Shen, Z. X., Chen, G. C., Kang, Y. M., Zou, S. C., Zhang, L. Z., Qi, S. H., Dai, M. H., Cheng, Y., and

ACPD
14, 435–469, 2014

Hu, K.: Spatial and seasonal distributions of carbonaceous aerosols over China, J. Geophys. Res., 112, D22S11, doi:10.1029/2006JD008205, 2007.

Cheng, Y. F., Wiedensohler, A., Eichler, H., Heintzenberg, J., Tesche, M., Ansmann, A., Wendisch, M., Su, H., Althausen, D., Herrmann, H., Gnauk, T., Brüggemann, E., Hu, M., and Zhang, Y. H.: Relative humidity dependence of aerosol optical properties and direct radiative forcing in the surface boundary layer at Xinken in Pearl River Delta of China: an observation based numerical study, Atmos. Environ., 42, 6373–6397, 2008a.

Cheng, Y. F., Wiedensohler, A., Eichler, H., Su, H., Gnauk, T., Brüggemann, E., Herrmann, H., Heintzenberg, J., Slanina, J., Tuch, T., Hu, M., and Zhang, Y. H.: Aerosol optical properties and related chemical apportionment at Xinken in Pearl River Delta of China, Atmos. Environ., 42, 6351–6372, 2008b.

Fountoukis, C. and Nenes, A.: ISORROPIA II: a computationally efficient thermodynamic equilibrium model for K^+-Ca^{2+}-Mg^{2+}-NH_4^+-Na^+-SO_4^{2-}-NO_3^--Cl^--H_2O aerosols, Atmos. Chem. Phys., 7, 4639–4659, doi:10.5194/acp-7-4639-2007, 2007.

Gysel, M., Weingartner, E., Nyeki, S., Paulsen, D., Baltensperger, U., Galambos, I., and Kiss, G.: Hygroscopic properties of water-soluble matter and humic-like organics in atmospheric fine aerosol, Atmos. Chem. Phys., 4, 35–50, doi:10.5194/acp-4-35-2004, 2004.

Lin, Z. J., Tao, J., Chai, F. H., Fan, S. J., Yue, J. H., Zhu, L. H., Ho, K. F., and Zhang, R. J.: Impact of relative humidity and particles number size distribution on aerosol light extinction in the urban area of Guangzhou, Atmos. Chem. Phys., 13, 1115–1128, doi:10.5194/acp-13-1115-2013, 2013.

Liu, X. G., Cheng, Y. F., Zhang, Y. H., Jung, J. S., Sugimoto, N., Chang, S. Y., Kim, Y. J., Fan, S. J., and Zeng, L. M.: Influences of relative humidity and particle chemical composition on aerosol scattering properties during the 2006 PRD campaign, Atmos. Environ., 42, 1525–1536, 2008.

Liu, X. G., Zhang, Y. H., Jung, J. S., Gu, J. W., Li, Y. P., Guo, S. C., Chang, S., Yue, D. L., Lin, P., Kim, Y. J., Hu, M., Zeng, L. M., and Zhu, T.: Research on the hygroscopic properties of aerosols by measurement and modeling during CAREBeijing-2006, J. Geophys. Res.-Atmos., 114, D00G16, doi:10.1029/2008JD010805, 2009.

Malm, W. C., Day, D. E., Kreidenweis, S. M., Collett, J. L., and Lee, T.: Humidity-dependent optical properties of fine particles during the Big Bend Regional Aerosol and Visibility Observational Study, J. Geophys. Res., 108, 4279, doi:10.1029/2002JD002998, 2003.

ACPD
14, 435–469, 2014

Pitchford, M., Maim, W., Schichtel, B., Kumar, N., Lowenthal, D., and Hand, J.: Revised algorithm for estimating light extinction from IMPROVE particle speciation data, J. Air Waste Manag., 57, 1326–36, 2007.
Seinfeld, J. H. and Pandis, S. N.: Atmospheric Chemistry and Physics: From Air Pollution to Climate Change, 2nd edn., John Wiley and Sons Inc., New York, 2006.
Tang, I. N.: Chemical and size effects of hygroscopic aerosols on light scattering coefficients, J. Geophys. Res., 101, 19245–19250, doi:10.1029/96JD03003, 1996.
Tang, I. N. and Munkelwitz, H. R.: Water activities, densities, and refractive indices of aqueous sulfates and sodium nitrate droplets of atmospheric importance, J. Geophys. Res., 99, 18801–18808, doi:10.1029/94JD01345, 1994.
Tang, I. N., Tridico, A. C., and Fung, K. H.: Thermodynamic and optical properties of sea salt aerosols, J. Geophy. Res., 102, 23269–23275, doi:10.1029/97JD01806, 1997.
Tao, J., Ho, K. F., Chen, L. G., Zhu, L. H., Han, J. L., and Xu, Z. C.: Effect of chemical composition of $PM_{2.5}$ on visibility in Guangzhou, China, 2007 spring, Particuology, 7, 68–75, doi:10.1016/j.partic.2008.11.002, 2009.
Tao, J., Cao, J. J., Zhang, R. J., Zhu, L. H., Zhang, T., Shi, S., and Chan, C. Y.: Reconstructed light extinction coefficients using chemical compositions of $PM_{2.5}$ in winter in Urban Guangzhou, China, Adv. Atmos. Sci., 29, 359–368, doi:10.1007/s00376-011-1045-0, 2012.
Tao, J., Zhang, L. M., Ho, K. F., Zhang, R. J., Lin, Z. J., Zhang, Z. S., Lin, M., Cao, J. J., Liu, S. X., and Wang, G. H.: Impact of $PM_{2.5}$ chemical compositions on aerosol light scattering in Guangzhou – the largest megacity in South China, Atmos. Res., 135–136, 48–58, doi:10.1016/j.atmosres.2013.08.015, 2014.
Wexler, A. S. and Clegg, S. L.: Atmospheric aerosol models for systems including the ions H^+, NH_4^+, Na^+, SO_4^{2-}, NO_3^-, Cl^-, Br^-, and H_2O, J. Geophys. Res.-Atmos., 107, ACH 14-1–ACH 14-14, 2002.
Wu, D., Tie, X. X., Li, C. C., Ying, Z. M., Lau, K. H., Huang, J., Deng, X. J., and Bi, X. Y.: An extremely low visibility event over the Guangzhou region: a case study, Atmos. Environ., 39, 6568–6577, 2005.
Wu, D., Mao, J. T., and Deng, X. J.: Black carbon aerosols and their radiative properties in the Pearl River Delta region, SCIENCE CHINA Earth Sciences, 52, 1152, doi:10.1007/s11430-009-0115-y, 2009.
Xing, L., Fu, T.-M., Cao, J. J., Lee, S. C., Wang, G. H., Ho, K. F., Cheng, M.-C., You, C.-F., and Wang, T. J.: Seasonal and spatial variability of the OM/OC mass ratios and high regional

ACPD
14, 435–469, 2014

correlation between oxalic acid and zinc in Chinese urban organic aerosols, Atmos. Chem. Phys., 13, 4307–4318, doi:10.5194/acp-13-4307-2013, 2013.

Xu, J., Bergin, M. H., Yu, X., Liu, G., Zhao, J., Carrico, C. M., and Baumann, K.: Measurement of aerosol chemical, physical and radiative properties in the Yangtze delta region of China, Atmos. Environ., 36, 161–173, doi:10.1016/S1352-2310(01)00455-1, 2002.

Zhang, L., Vet, R., Wiebe, A., Mihele, C., Sukloff, B., Chan, E., Moran, M. D., and Iqbal, S.: Characterization of the size-segregated water-soluble inorganic ions at eight Canadian rural sites, Atmos. Chem. Phys., 8, 7133–7151, doi:10.5194/acp-8-7133-2008, 2008.

Zhang, Y. H., Hu, M., Zhong, L. J., Wiedensohler, A., Liu, S. C., Andreae, M. O., Wang, W., and Fan, S. J.: Regional integrated experiments on air quality over Pearl River Delta 2004 (PRIDE-PRD2004): overview, Atmos. Environ., 42, 6157–6173, doi:10.1016/j.atmosenv.2008.03.025, 2008.

Zhang, Z. S., Engling, G., Chan, C. Y., Yang, Y. H., Lin, M., Shi, S., He, J., Li, Y. D., and Wang, X. M.: Determination of isoprene-derived secondary organic aerosol tracers (2-methyltetrols) by HPAEC-PAD: results from size-resolved aerosols in a tropical rainforest, Atmos. Environ., 70, 468–476, doi:10.1016/j.atmosenv.2013.01.020, 2013.

ACPD
14, 435–469, 2014

Table 1. Summary of instrumental details.

Property	Instrument	Variable	Available	Output Time-resolution	Uncertainty %	RH condition	Aggregated Time-resolution
Particle Sampling	cascade impactor	Particles mass	May Jun Nov Dec 2010	23.5 h	1.08[a]	ambient	23.5 h
Chemical Analysis	Ion Chromatography and Carbon Analyzer	Water-soluble ions and OC/EC mass	May Jun Nov Dec 2010	23.5 h	2.49[a]	~ 40 % in laboratory	23.5 h
Meteorology	VAISALA QMH102	Temperature	Mar 2008 to Dec 2010	0.5 h	2.40[b]	ambient	1 h and 23.5 h
		Relative Humidity	Mar 2008 to Dec 2010	0.5 h	3.04[b]	ambient	1 h and 23.5 h
		Air Pressure	Mar 2008 to Dec 2010	0.5 h	0.03[b]	ambient	1 h and 23.5 h
	VAISALA PWD22	Air Visibility	Mar 2008 to Dec 2010	0.5 h	5.00[b]	ambient	1 h and 23.5 h
Gaseous pollutant	Thermo 42i	mass concentration of NO_2	Mar 2008 to Dec 2010	5 min	1.00[c]	ambient	1 h and 23.5 h
Aerosol optical property	Magee AE-31	mass concentration of BC (880 nm)	Mar 2008 to Dec 2010	5 min	5.00[d]	~ 40 % drying tube	1 h and 23.5 h
	TSI 3563	scattering coefficient (550 nm)	Mar 2008 to Apr 2010	1 min	2.30[e]	inner heating	1 h and 23.5 h

[a] Paper (Lin et al., 2013).
[b] Users' manual of the VAISALA weather station and PWD 22.
[c] Paper (Liu et al., 2009).
[d] Measurements and Analytical Specifications in HERO database of USEPA.
[e] Paper (Cheng et al., 2008b).

ACPD
14, 435–469, 2014

Table 2. Potential major compounds with respect to the abundance of SO_4^{2-}.

Abundance of SO_4^{2-}	Potential Major Compounds
SO_4^{2-} rich	$NaHSO_4$, NH_4HSO_4, $KHSO_4$, K_2SO_4, $MgSO_4$, Na_2SO_4, $(NH_4)_2SO_4$, H_2SO_4, $CaSO_4$
SO_4^{2-} less rich	K_2SO_4, $MgSO_4$, Na_2SO_4, $(NH_4)_2SO_4$, H_2SO_4, $CaSO_4$, $NaNO_3$, NaCl, NH_4NO_3, NH_4Cl, $Ca(NO_3)_2$, $CaCl_2$, $Mg(NO_3)_2$, $MgCl_2$, KNO_3, KCl
SO_4^{2-} poor	$NaNO_3$, NaCl, NH_4NO_3, NH_4Cl, $Ca(NO_3)_2$, $CaCl_2$, $Mg(NO_3)_2$, $MgCl_2$, KNO_3, KCl

ACPD
14, 435–469, 2014

Table 3. Density and optical refractive index of chemical component.

Species	ρ	m (= $n + ki$) n	k	Species	ρ	m (= $n + ki$) n	k
NH_4HSO_4	1.780	1.473	0.000	$KHSO_4$	2.245	1.480	0.000
$(NH_4)_2SO_4$	1.760	1.530	0.000	$Ca(NO_3)_2$	2.504	1.530	0.000
$NaHSO_4$	2.476	1.460	0.000	$CaCl_2$	2.150	1.520	0.000
Na_2SO_4	2.680	1.480	0.000	$Mg(NO_3)_2$	2.020	1.510	0.000
NH_4NO_3	1.725	1.554	0.000	$MgCl_2$	2.325	1.540	0.000
$NaNO_3$	2.261	1.587	0.000	KNO_3	2.110	1.504	0.000
NH_4Cl	1.527	1.639	0.000	KCl	1.980	1.490	0.000
NaCl	2.160	1.544	0.000	HNO_3[a]	1.504	1.396	0.000
K_2SO_4	2.660	1.490	0.000	HCl[a]	1.198	1.342	0.000
$MgSO_4$	2.660	1.560	0.000	Water	1.000	1.333	0.000
$CaSO_4$	2.610	1.570	0.000	POM	1.400	1.550	0.001
H_2SO_4	1.840	1.430	0.000	EC	1.500	1.800	0.540

[a] Updated in current study.

ACPD
14, 435–469, 2014

Table 4. Statistical result of fundamental data in current study.

Variable	Unit	May–Jun 2010 (23.5 h average)	Nov–Dec 2010 (23.5 h average)	Mar 2008–Dec 2010 (1 h average)
$b_{sp,mea}$	Mm^{-1}	532.4 ± 292.4	485.6 ± 199.1	529.5 ± 496.8
$b_{sp,cal}$ [a]	Mm^{-1}	–	–	347.0 ± 280.6
RH_{vis}		0.71 ± 0.09	0.48 ± 0.09	66.9 ± 17.2
RH_{nep}		–	–	53.3 ± 14.5
$b_{ag,mea}$	Mm^{-1}	12.4 ± 5.5	11.9 ± 3.6	11.0 ± 6.2
$b_{sg,mea}$	Mm^{-1}	11.1 ± 0.1	11.4 ± 0.1	11.3 ± 0.3
$b_{ap,mea}$	Mm^{-1}	35.9 ± 22.9	39.8 ± 15.7	53.9 ± 39.2
Na^+	$\mu g\,m^{-3}$	2.20 ± 1.86	0.91 ± 0.47	–
SO_4^{2-}	$\mu g\,m^{-3}$	13.53 ± 5.74	16.60 ± 5.11	–
NH_4^+	$\mu g\,m^{-3}$	5.36 ± 3.15	6.84 ± 2.33	–
NO_3^+	$\mu g\,m^{-3}$	9.02 ± 5.36	9.67 ± 5.81	–
Cl^-	$\mu g\,m^{-3}$	1.72 ± 0.64	1.03 ± 1.02	–
Ca^{2+}	$\mu g\,m^{-3}$	1.56 ± 0.56	1.63 ± 0.57	–
K^+	$\mu g\,m^{-3}$	0.57 ± 0.32	1.32 ± 0.39	–
Mg^{2+}	$\mu g\,m^{-3}$	0.23 ± 0.08	0.17 ± 0.06	–
OC	$\mu g\,m^{-3}$	9.46 ± 3.66	14.30 ± 4.38	–
EC	$\mu g\,m^{-3}$	4.02 ± 3.81	4.53 ± 2.56	–

[a] without the $f_{sp}(RH)$ correction.

ACPD
14, 435–469, 2014

Table 5. Comparison between Eqs. (8) and (10).

Index	Exponent of the curve	$f_{sp,int}$	$f_{sp,ext}$	$f_{sp,cs}$
RSDA	$a \cdot RH$	0.0803	0.0911	0.0761
	$a \cdot (RH + b_{varying})$	0.3145	0.3687	0.3031
	$a \cdot (RH + b_{constant})$	0.0831	0.0947	0.0783
MATR	$a \cdot RH$	0.8498	0.7081	0.7335
	$a \cdot (RH + b_{varying})$	0.0726	0.0638	0.0828
	$a \cdot (RH + b_{constant})$	0.0917	0.0923	0.0927
MIRV	$a \cdot RH$	0.9558	0.9525	0.9583
	$a \cdot (RH + b_{varying})$	0.9937	0.9939	0.9926
	$a \cdot (RH + b_{constant})$	0.9924	0.9877	0.9919

ACPD
14, 435–469, 2014

Table 6. Parameters of f_{sp}(RH) curve related to mixing state.

Mixing state	*a*	*b*
Internal Mixed	0.1650	1.90
External Mixed	0.1647	1.65
Core–Shell	0.2021	1.45

ACPD
14, 435–469, 2014

Fig. 1. Satellite photo of the observation site and surroundings (from Google Earth).

ACPD
14, 435–469, 2014

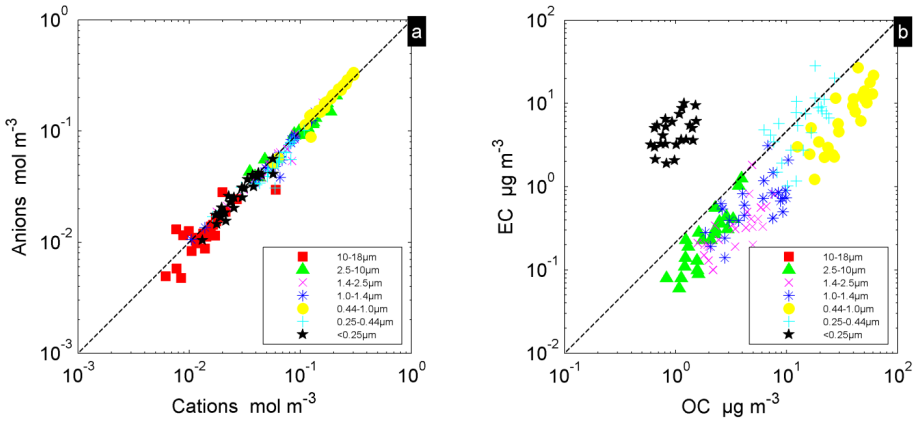

Fig. 2. The measurement data collected during May, June, November and December in 2010: **(a)** ionic charge balance between anions and cations, and **(b)** mass concentrations of OC vs. EC.

ACPD
14, 435–469, 2014

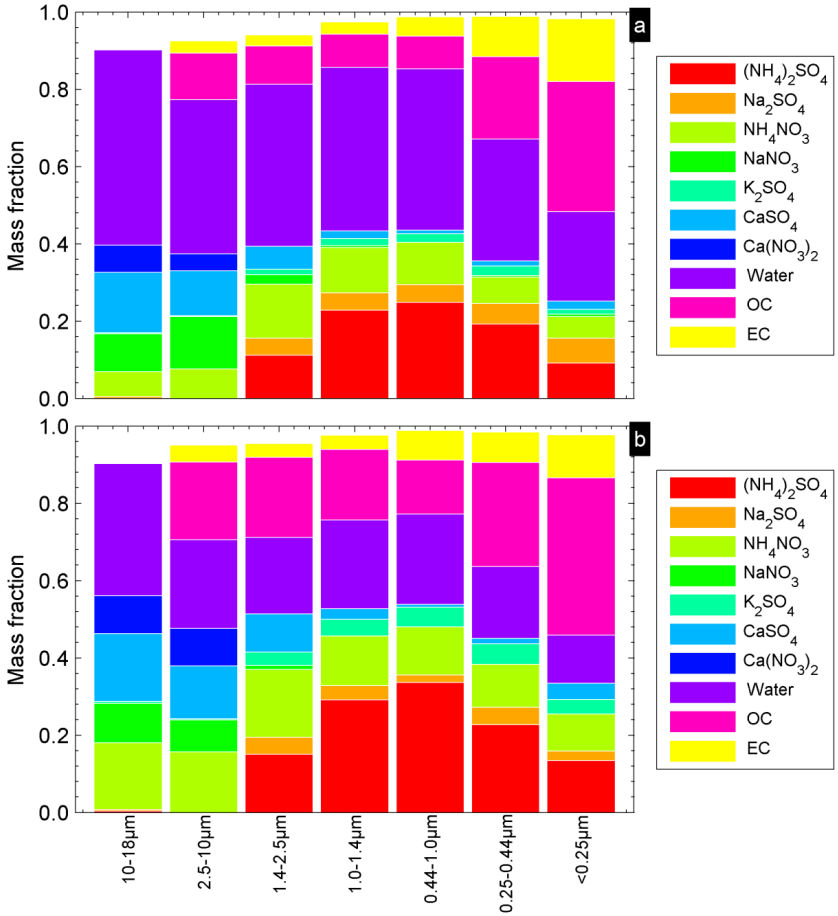

Fig. 3. Reconstructed mass fractions of major chemical constituents in different particle size stages in wet **(a)** and dry **(b)** seasons.

ACPD
14, 435–469, 2014

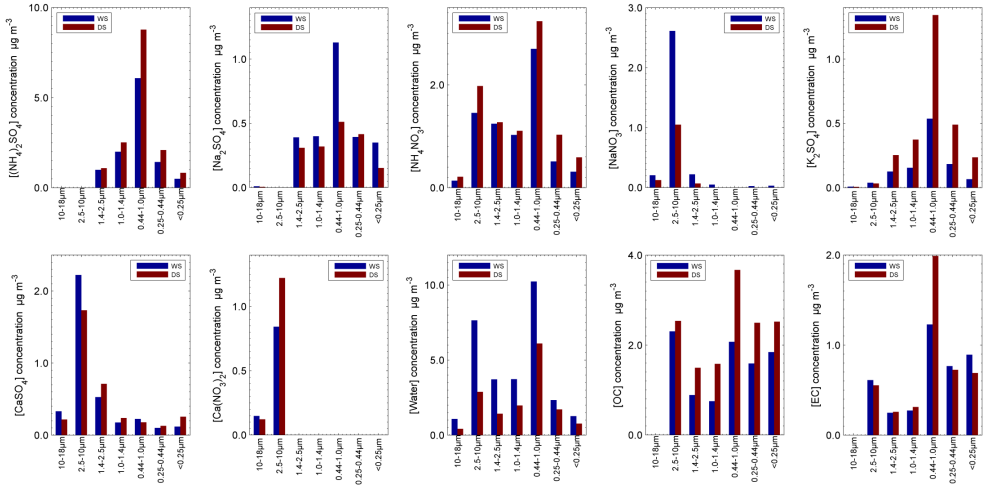

Fig. 4. Reconstructed mass size distributions of major chemical constituents.

ACPD
14, 435–469, 2014

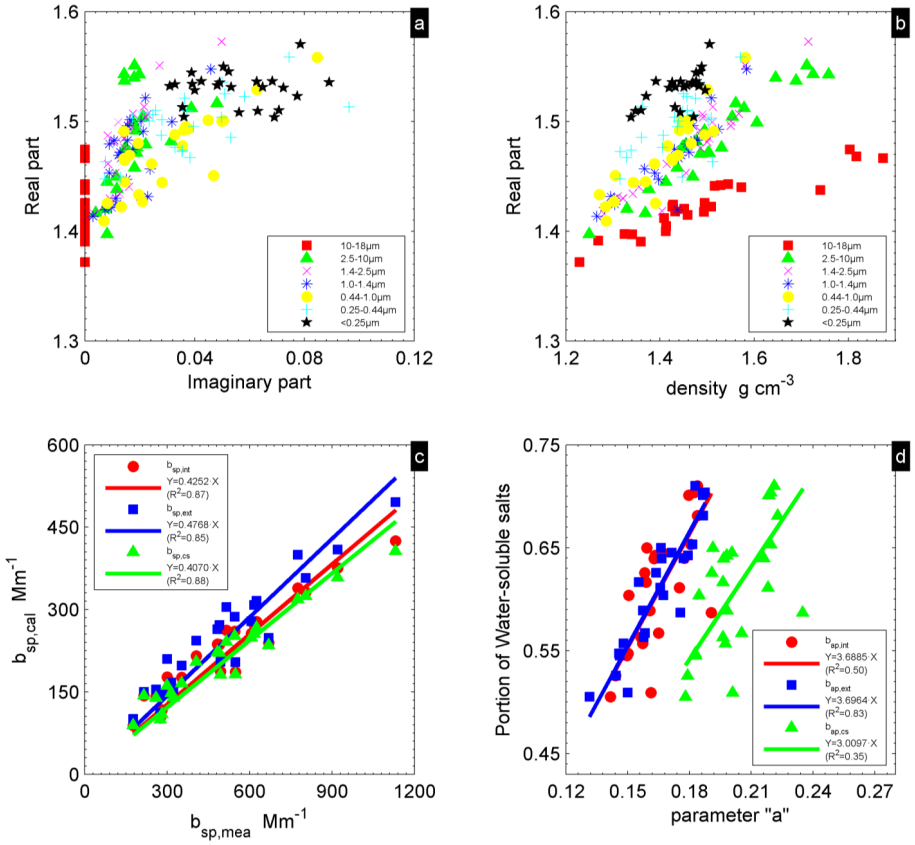

Fig. 5. (a) The imaginary vs. real part of optical refractive index; **(b)** the real part of optical refractive index vs. particle density; **(c)** Mie model calculated b_{sp} with three types of mixed aerosols vs. visibility derived b_{sp}; **(d)** water-soluble fraction of aerosols vs. parameter "*a*" of f_{sp}(RH) formula.

ACPD
14, 435–469, 2014

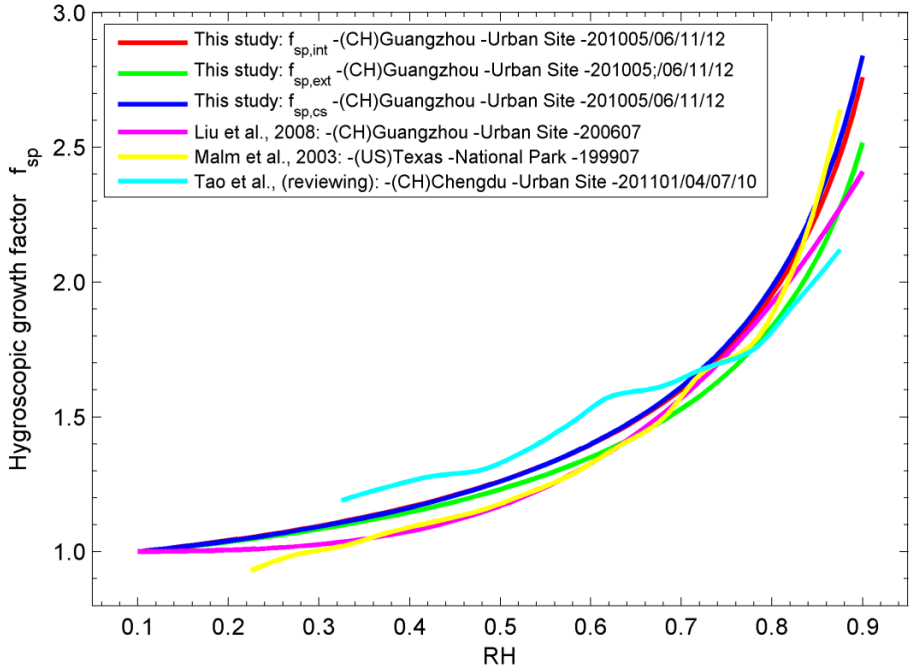

Fig. 6. Comparison of f_{sp}(RH) curve determined in present study with those from literatures.

ACPD
14, 435–469, 2014

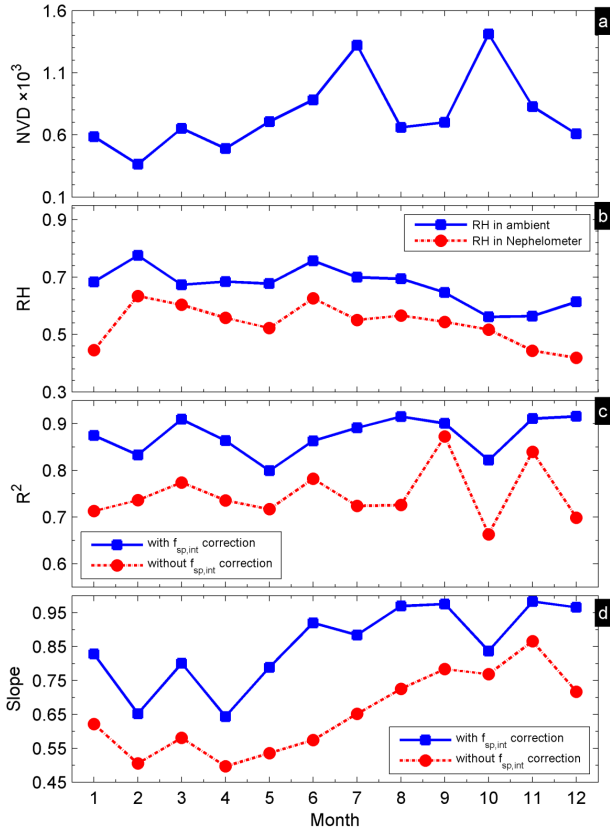

Fig. 7. (a) Numbers of available data in linear regression between Nephelometer measured b_{sp} and visibility derived b_{sp}; **(b)** comparison between RH in ambient and that inside Nephelometer; **(c)** value of R^2 in linear regression between Nephelometer measured b_{sp} and visibility derived b_{sp}; **(d)** value of slope in linear regression between Nephelometer measured b_{sp} and visibility derived b_{sp}.

ACPD
14, 435–469, 2014

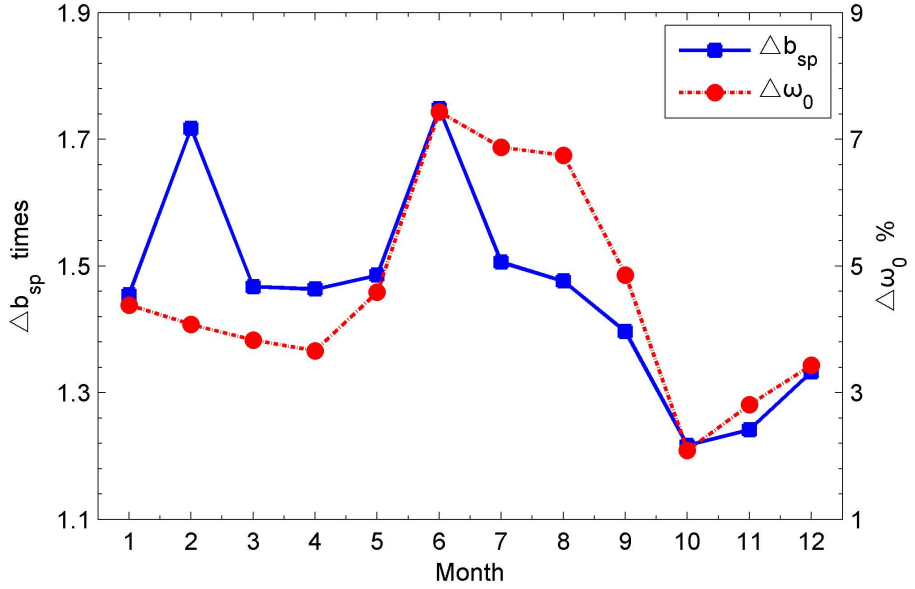

Fig. 8. Contribution of RH to b_{sp} and ω_0 enhancement.

ACPD
14, 435–469, 2014